Optimal Control of Molecular Spin Qudits

Alberto Castro [1,2,*] Adrián García Carrizo,[2] Sebastián Roca,[3,4] David Zueco,[3,4] and
Fernando Luis [3,4]

[1] *ARAID Foundation, Avenida de Ranillas 1, Zaragoza 50018, Spain*

[2] *Institute for Biocomputation and Physics of Complex Systems (BIFI) of the University of Zaragoza, Edificio de Institutos Universitarios de Investigación, Calle Mariano Esquillor, Zaragoza 50018, Spain*

[3] *Instituto de Nanociencia y Materiales de Aragón (INMA), CSIC-Universidad de Zaragoza, Pedro Cerbuna 12, Zaragoza 50009, Spain*

[4] *Departamento de Física de la Materia Condensada, Universidad de Zaragoza, Zaragoza 50009, Spain*

We demonstrate, numerically, the possibility of manipulating the spin states of molecular nanomagnets with shaped microwave pulses designed with quantum optimal control theory techniques. The state-to-state or full gate transformations can be performed in this way in shorter times than using simple monochromatic resonant pulses. This enhancement in the operation rates can therefore mitigate the effect of decoherence. The optimization protocols and their potential for practical implementations are illustrated by simulations performed for a simple molecular cluster hosting a single Gd^{3+} ion. Its eight accessible levels (corresponding to a total spin $S = 7/2$) allow encoding an eight-level qudit or a system of three coupled qubits. All necessary gates required for universal operation can be obtained with optimal pulses using the intrinsic couplings present in this system. The application of optimal control techniques can facilitate the implementation of quantum technologies based on molecular spin qudits.

I. INTRODUCTION

A crucial challenge for the development of quantum simulation and quantum computation is to scale up computational power while keeping the processor robust against noise and limiting the complexity of control lines and electronics [1–3]. A promising strategy is to replace qubits with d-dimensional ($d > 2$) quantum systems, or qudits [4–6], as the elementary building blocks of the quantum architecture. The ability to integrate nontrivial operations in a single physical system helps simplify some quantum algorithms [7–9]. In addition, it can also facilitate their implementation by reducing the number of nonlocal operations, i.e., those connecting different parts of the circuit.

Qudits have been realized with the multiple quantum states of diverse physical systems, including photons [10], trapped ions [11], impurity nuclear spins in semiconductors [12], and superconducting circuits [13]. Here, we focus on a special class of systems, molecular nanomagnets [14–18] (see Fig. 1 for an illustrative example). These are coordination or supramolecular complexes that consist of a magnetic core surrounded by a shell of organic ligand molecules. Chemistry offers nearly unbound possibilities for the design of spin qudits based on these molecules. The combination of one or several $S > 1/2$ transition metals or lanthanide ions with sufficiently weak magnetic anisotropy and/or exchange interactions gives rise to a number of low-lying magnetic levels. For suitably chosen molecular structures, these levels are unequally spaced, making transitions between them addressable via microwave resonant pulses. And nuclear spin states of the metal ions provide additional resources [21–25].

Examples of molecular-based electronic and electronuclear spin qudits, with dimension d ranging from 4 up to 64, have recently been reported [19,21–31]. In addition, there have been proposals for exploiting their multiple states to specific applications. Relevant examples are the digital quantum simulation of spin-boson models [32], where the qudit encodes boson states, and the implementation of quantum error correction codes [31,33,34]. The latter is particularly promising, as embedding in each basic unit, in this case a molecule, a suitably designed protection against its specific decoherence sources might represent a huge competitive advantage. Besides, the functionalities need not be defined *a priori*. When the allowed transitions between different qudit states form a universal set, these systems can be regarded as microscopic size universal processors (or NISQs) [18,19,24,29,30,35].

However, decoherence remains a serious limitation for fully unleashing the potential of these otherwise very appealing systems. Even though some specifically
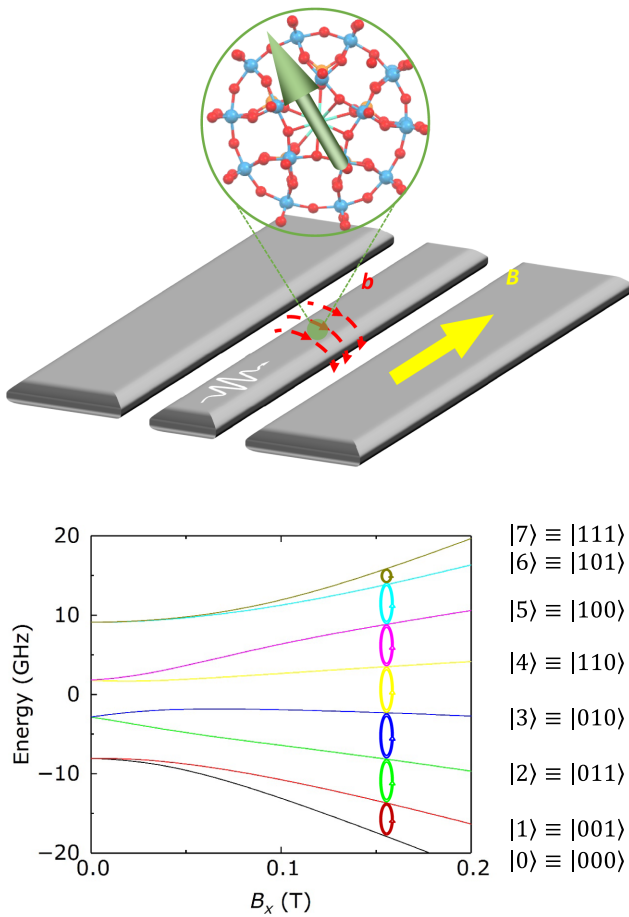
FIG. 1. Top: schematic image of a molecular spin subject to a static magnetic field $\vec{B}$ and to an arbitrarily shaped microwave magnetic field $\vec{b}$, here generated by a transmission line. Bottom: spin energy levels of the GdW$_{30}$ polyoxometalate cluster [19,20], whose structure is shown in the top. The eight spin states, associated with the $S = 7/2$ spin of the central Gd^{3+} ion, enable encoding a $d = 8$ qudit or three qubits. The colored circular arrows mark the seven transitions that can be implemented by means of resonant monochromatic pulses.

designed molecular spin qubits show remarkably long coherence times T_2 [36,37], decoherence tends to increase for higher spin or molecules with a higher number of magnetic atoms. A sequence of necessarily imperfect gates might become impractically long as compared to T_2, leading to large error rates. In the paradigmatic example of a qudit-based quantum error protocol, such effects can completely overcome the gain brought about by the code itself [31,33]. Clearly, this calls for more efficient methods to carry out such operations.

In this work, we consider the possibility of applying quantum optimal control theory (QOCT) techniques [38,39] to mitigate some of the limitations associated with the use of monochromatic resonant pulses. The use of QOCT for the manipulation of spin systems was

demonstrated in the field of nuclear magnetic resonance [40–44]. This theory allows designing more complex pulses in order to find the temporal shape of the external perturbation that makes the evolution operator equal to a predefined gate, as shown by Palao and Kosloff [45]. Numerous later calculations employing similar schemes have been reported [46–53]. We present here a modification of the method that allows for the use of arbitrarily parameterized pulses, which permit one to seamlessly impose constraints that match the experimental constraints. We illustrate its application to the efficient control of molecular spin qudits by performing numerical simulations on a $d = 8$ qudit encoded in the $S = 7/2$ spin states of a simple molecular cluster hosting a Gd^{3+} ion (Fig. 1) [20], for which a universal set of operations is realized experimentally [19]. We have parameterized the pulses using a range of different frequencies, and limited the amplitude of each component (since otherwise the optimizations tend to favor high intensity solutions that may be experimentally inaccessible and, moreover, would reduce the coherence times via the excitation of unwanted levels). The purpose is to assess the expected gains of using a multifrequency setup, compared to the usual route to gate construction through simple monochromatic rotations.

The manuscript is organized as follows. In Sec. II we introduce the spin Hamiltonian describing the qudit, discuss standard control techniques based on monochromatic resonant pulses and its limitations in terms of operation speeds and fidelities, and describe the optimization methodology used in this work. Section III shows results obtained by these two methods and discusses their differences. Finally, Sec. IV summarizes the conclusions and future prospects derived from these results.

II. MODEL AND METHODOLOGY

A. Spin Hamiltonian: definition of qudit basis states

We consider a situation similar to that shown schematically in Fig. 1, where a molecular spin qudit is tuned by an external magnetic field $\vec{B}$ and controlled by a time-dependent perturbation able to induce transitions between its different states. The underlying physics can be described by the spin Hamiltonian

$$\hat{H} = \hat{H}_{\text{ZF}} + \hat{H}_{\text{Zeeman}} + \hat{H}_{\text{TD}}, \tag{1}$$

where $\hat{H}_{\text{ZF}}$ is the zero-field spin Hamiltonian of the isolated molecule, $\hat{H}_{\text{Zeeman}}$ is the Zeeman interaction with $\vec{B}$, and $\hat{H}_{\text{TD}}$ is a time-dependent control term. In general, $\hat{H}_{\text{ZF}}$ can be quite complex and include the single-ion anisotropy of the magnetic ions forming the molecular core, their mutual exchange and dipolar interactions, as well as the hyperfine couplings to the nuclear spins. Yet, quite often this Hamiltonian can be simplified. This is the case when dealing with mononuclear molecules, hosting one metal ion, or when

exchange interactions are sufficiently strong to ensure that only states with the lowest-energy total spin value S are significantly populated at the relevant temperatures. The spin response can then be well approximated with the help of a "giant spin" approximation [14,54]. In this work, we use the expressions

$$\hat{H}_{ZF} = D\left[\hat{S}_z^2 - \frac{1}{3}S(S+1)\right] + E(\hat{S}_x^2 - \hat{S}_y^2), \quad (2)$$

$$\hat{H}_{Zeeman} = -g\mu_B\vec{B}\hat{\vec{S}}, \quad (3)$$

where S is the spin quantum number of the molecule, $(\hat{S}_x, \hat{S}_y, \hat{S}_z)$ are the spin operators, D and E are magnetic anisotropy constants, g is the spin g factor, and μ_B is the Bohr magneton. These expressions accurately describe the GdW$_{30}$ molecular spin qudit, which we use in Sec. III below to illustrate the potential of QOCT techniques. In particular, the uniaxial magnetic anisotropy DS_z^2 provides the level anharmonicity that is required to properly address individual transitions between the qudit states. Yet, the methodology is general and could be applied to more complex versions of the spin Hamiltonian adapted to diverse implementations (e.g., those including weakly coupled electronic spins or a combination of nuclear and electronic spin states).

The last term in Eq. (1) provides the ability to control the quantum spin states. As with the static terms, for the sake of simplicity, we use the form

$$\hat{H}_{TD} = -g\mu_B f(t)\vec{b}\hat{\vec{S}}, \quad (4)$$

which corresponds to a time-dependent version of the Zeeman interaction term (3). This Hamiltonian describes the most common spin control techniques, based on electron paramagnetic resonance methods, in which the absorption of this signal is the crucial observable. In recent times, it has been shown that spin qubits, including those in molecules, can also be manipulated by means of electric field pulses [55,56]. In this case, the time-dependent perturbation introduces a modulation of the crystal field and the magnetic anisotropy terms associated with it. Again, the methods described below are easily adaptable to these situations.

B. Coherent control via monochromatic resonant pulses

Often, the temporal shape is a simple monochromatic term, e.g.,

$$f(t) = \lambda\cos(\omega t + \phi)\Pi_{t_0}^{t_f}(t), \quad (5)$$

where the amplitude is determined by λ, and $\Pi_{t_0}^{t_f}$ is the rectangular function that is equal to one if $t_0 \leq t \leq t_f$,

and zero otherwise (in reality, of course, the ramp up and down at t_0 and t_f are not abrupt). If the frequency is chosen to be close to one of the resonances, and the amplitude is low enough, the rotating wave approximation may be applied, and the effect of these pulses can be worked out analytically: if j, k are the two levels linked by the resonance (let us assume a perfect resonance, and that all other frequencies are well separated), the evolution operator $\hat{U}(t)$ is

$$\hat{U}(t) = \hat{R}_{\vec{n}}^{(jk)}(\theta) \oplus \hat{I}^{(\overline{jk})}. \quad (6)$$

This expression assumes the interaction representation, and, in order to simplify the notation, we have set $t_0 = 0$. The superindex (jk) on the two-dimensional *rotation* operator $\hat{R}_{\vec{n}}^{(jk)}(\theta)$ means that it acts on the subspace spanned by the j, k levels, whereas the rest of the levels are unaffected ($\hat{I}^{(\overline{jk})}$ is the identity in all but the j, k levels). Within the basis spanned by the two states, j, k, the rotation operator is given by

$$\hat{R}_{\vec{n}}(\theta) = \exp\left(-i\frac{\theta}{2}\vec{n}\cdot\hat{\vec{\sigma}}\right) \quad (7)$$

with $\hat{\vec{\sigma}}$ the vector of Pauli matrices. The rotation angle θ is $\lambda g\mu_B|\mu_{jk}|t$, where $\mu_{jk} = \langle j|\vec{b}\hat{\vec{S}}|k\rangle$ is the coupling matrix element, and $\vec{n}$ is the unit vector:

$$\vec{n} = (\cos(\arg\mu_{jk} + \phi), -\sin(\arg\mu_{jk} + \phi), 0). \quad (8)$$

The choice of ϕ determines the rotation axis: if $\phi = -\arg\mu_{jk}$, we have a $R_X(\theta)$ rotation; if $\phi = -\arg\mu_{jk} - \pi/2$, we have a $R_Y(\theta)$ rotation. We cannot have direct $R_Z(\theta)$ rotations, but they can however be built by combinations of the former two. We recall that here X, Y, Z do not refer to any spatial direction, but to the Pauli matrices defined in the basis spanned by the states j, k.

Let us consider $R_X(\theta)$ rotations in the following. By adjusting the total pulse time t_f, one selects the angle θ and, for example, performs a π rotation, i.e., if

$$t_f = t_\pi^\lambda = \frac{\pi}{\lambda g\mu_B|\mu_{jk}|}, \quad (9)$$

the rotation transforms the j state into the k state and vice versa:

$$\hat{R}_X(\pi) = -i\begin{bmatrix} 0 & 1 \\ 1 & 0 \end{bmatrix}. \quad (10)$$

Note the presence of the $-i$ factor; it is an irrelevant global phase factor if we consider the (j, k) subspace as isolated, but it changes the phase with respect to the rest of the levels.

In order to use these qudits as quantum information units, however, one needs the ability to perform arbitrary unitaries, and not only two-level rotations. Fortunately, by concatenation of several of these rotations, one may construct arbitrary unitaries in any 2^n-level system [18,19,24, 30,57,58] (cf. the Appendix for details). The necessary sequences, as we will show later in an example, may be long.

Furthermore, another problem that cannot be remedied is the approximate character of all previous expressions that rely on the weakness of the perturbation amplitude λ, thus avoiding the possibility of arbitrarily speeding up the process by increasing that amplitude. If we require a minimum fidelity for the $|j\rangle \to |k\rangle$ transformations then a minimum amount of time is necessary.

C. Quantum optimal control theory

The previous arguments reveal an intrinsic limitation of monochromatic pulses for the creation of fast quantum gates, which may be further complicated by the presence of experimental constraints, i.e., the inability to increase the magnetic field intensities. In order to create faster gates, one may attempt to use more complex temporal shapes, i.e., combine various frequencies. We therefore wonder how this possibility may help the control of molecular spin qudits, i.e., whether operation times can be made substantially shorter than the coherence times. For this purpose, we have applied QOCT. We summarize in the following the method and the basic equations that we have employed.

QOCT can be formulated in two different ways. One, the optimization of "point-to-point" or "state-to-state" transitions, i.e., the transfer of one particular initial state to a final one. Two, a "universal" optimization, i.e., the control of the full evolution operator of the process, which implies the full control of the evolution of any state. This last formulation is the one that one needs in order to find external couplings capable of generating quantum gates, and is therefore the one that we have focused on in this work. For this reason, this is the one that we describe below. However, since we also describe some state-to-state optimizations in the results section, we will also write at the end of this section the necessary equations for those calculations.

We consider that the time-dependent pulse-shape function $f(t)$ alluded to above is parameterized with a set of values $u_0, \ldots, u_M \equiv u$: i.e., $f = f(u; t)$. The evolution of the system is then determined by the Hamiltonian

$$\hat{H}(u; t) = \hat{H}_0 + f(u; t)\hat{V}, \qquad (11)$$

where $\hat{H}_0 = \hat{H}_{\text{ZF}} + \hat{H}_{\text{Zeeman}}$ and $\hat{V} = -g\mu_B \hat{\vec{S}}\vec{b}$.

The evolution operator $\hat{U}(u; t)$ is thus also determined by u. In the interaction representation it evolves according to

$$i\frac{\partial}{\partial t}\hat{U}(u; t) = f(u, t)\hat{\tilde{V}}(t)U(u; t), \qquad (12)$$

$$\hat{U}(u; 0) = \hat{I}, \qquad (13)$$

where $\hat{\tilde{V}}(t) = \exp(it\hat{H}_0)\hat{V}\exp(-it\hat{H}_0)$.

The goal is to find a set of parameters $u^{(0)}$ such that the evolution operator is equal—or equivalent—to a given target gate $\hat{U}_G$: $\hat{U}(u^{(0)}, T) = e^{ia}\hat{U}_G$ for any irrelevant global phase a. In the QOCT framework, this is achieved by finding a set of parameters that leads to the maximization of a functional of the system evolution; in this case this can be done by defining this functional as

$$F(\hat{U}) = |\hat{U} \cdot \hat{U}_{\text{target}}|^2, \qquad (14)$$

where the dot product in the space of linear transformations that we have used is the Fröbenius product

$$\hat{A} \cdot \hat{B} = \frac{1}{d}\text{Tr}[\hat{A}^{\dagger}\hat{B}]. \qquad (15)$$

Here, d is the space dimension. The functional thus defined acquires its maximum value (one) when $\hat{U}$ is equal to the target gate, modulo a phase factor. Since, as mentioned above, the evolution is determined by the parameters u, the problem is reduced to the maximization of the function

$$G(u) = F[\hat{U}(u; t_f)]. \qquad (16)$$

Many possible algorithms exist for finding the maxima of multivariate functions such as G. Most of them require computing the gradient of the function (in addition to the function itself). Optimal control theory provides the mathematical tool to derive these gradients (essentially, Pontryagin's maximum principle [59]). For the case of our function G, the gradient is given by

$$\frac{\partial G}{\partial u_m}(u) = 2\text{Im}\int_0^{t_f} dt\frac{\partial f}{\partial u_m}(u; t)\hat{B}(u; t) \cdot (\hat{\tilde{V}}(t)\hat{U}(u; t)), \qquad (17)$$

where the *costate* $\hat{B}$ is defined by the equations

$$i\frac{\partial}{\partial t}\hat{B}(u; t) = f(u, t)\hat{\tilde{V}}(t)U(u; t), \qquad (18)$$

$$\hat{B}(u; t_f) = (\hat{U}_{\text{target}} \cdot \hat{U}(t_f))\hat{U}_{\text{target}}. \qquad (19)$$

Note that it is an equation of motion similar to the one that determines the evolution operator itself, except the boundary condition is given at the final time of the propagation t_f (it is a *final* condition, instead of an initial condition). In consequence, the computation of the gradient requires two

propagations: a forward propagation for $\hat{U}$ and a backward propagation for $\hat{B}$.

It remains to specify the parameterization of f, an important task that actually defines the set of allowed temporal shapes. This should be done with the experimental limitations in mind. In our case, we have used two parameterizations. The first one is a simple Fourier expansion

$$f(u,t) = f_{\text{Fourier}}(u,t) = \frac{1}{\sqrt{t_f}}u_0$$
$$+ \sum_{k=1}^{K}\left[u_{2k}\frac{2}{\sqrt{t_f}}\cos(\omega_k t) + u_{2k-1}\frac{2}{\sqrt{t_f}}\sin(\omega_k t) \right]. \tag{20}$$

The frequencies $\omega_k = 2\pi k/t_f$, $k = 1, \ldots, K$, have a maximum *cutoff* value at $2\pi K/t_f$ that must be chosen big enough to include the relevant natural frequencies of the spin qudit, but not so large that it cannot be handled experimentally. Some constraints have to be imposed on the allowed values for the parameters: the pulse amplitude must start and end at zero, $f(u,0) = f(u,t_f) = 0$, which translates into $\sum_{k=1}^{K} u_{2k} = 0$. We have also imposed a zero value for the average amplitude, $\int_0^{t_f} dt\, f(u,t) = 0$, which translates into $u_0 = 0$. Finally, the generated magnetic field cannot have arbitrary amplitudes. One way to constrain it is to set a maximum value

$$\left| \frac{2u_k}{\sqrt{t_f}} \right| b \leq b_{\max}. \tag{21}$$

These constraints ensure that each frequency component does not surpass a given amplitude $b_{\max}$. It does not ensure, however, that the microwave field, composed of the sum of all components, surpasses that threshold. Depending on the experimental setup, however, it may happen that the field cannot surpass a given bound at any time. We have forced this constraint by also implementing an alternative parameterization consisting of a transformation of the Fourier series:

$$f(u,t) = \Phi(f_{\text{Fourier}}(u,t)) \tag{22}$$

with

$$\Phi(x) = b_{\max}\frac{x}{1+|x|} \tag{23}$$

Of course, other similar transformation functions can be used that ensure $|\Phi(x)| \leq b_{\max}$. Using a parameterization such as this, there is no need to impose a bound on the values of $|u_k|$.

We now briefly summarize the relevant equations for the simpler problem of point-to-point optimization. Some

of the previous equations must then be replaced by other ones. In particular, the equation of motion to be controlled, instead of Eqs. (12) and (13), is Schrödinger's equation for a single state:

$$i\frac{\partial}{\partial t}|\psi(u;t)\rangle = f(u,t)\hat{\tilde{V}}(t)|\psi(u;t)\rangle, \tag{24}$$

$$|\psi(u;0)\rangle = |\psi^0\rangle. \tag{25}$$

Often, the objective is the population of a target state $|\psi_{\text{target}}\rangle$, in which case the functional to be maximized is defined as

$$F(\psi) = |\langle\psi|\psi_{\text{target}}\rangle|^2, \tag{26}$$

instead of that given in Eq. (14). Therefore, the problem boils down to the maximization of $G(u) = F(\psi(u,t_f))$. In this case, the gradient is given by

$$\frac{\partial G}{\partial u_m}(u) = 2\text{Im}\int_0^{t_f} dt\frac{\partial f}{\partial u_m}(u;t)\langle\chi(u;t)|\hat{\tilde{V}}(t)|\psi(u;t)\rangle, \tag{27}$$

where the *costate* $|\chi(u;t)\rangle$ is now defined by

$$i\frac{\partial}{\partial t}|\chi(u;t)\rangle = f(u,t)\hat{\tilde{V}}(t)|\chi(u;t)\rangle, \tag{28}$$

$$|\chi(u;t_f)\rangle = \langle\psi_{\text{target}}|\chi(u;t)\rangle|\psi_{\text{target}}\rangle. \tag{29}$$

In order to implement both the QOCT equations for the gate optimization and for the point-to-point transitions, we have used the qutip code as a base [60,61]. We have, however, not employed the QOCT algorithms provided by this platform (at the time of writing this article), but used the gradient, computed as in Eq. (17), to feed our own QOCT code [62] that then utilizes a general purpose function optimization algorithm: the sequential least-squares quadratic programming algorithm [63] as implemented in the NLOPT library [64].

III. RESULTS

A. The GdW$_{30}$ molecular spin qudit

In order to explore the potential of QOCT for the control of spin qudits, we have chosen a system, GdW$_{30}$ [19,20], which is both well characterized and relatively simple. The molecular structure of this polyoxometalate cluster is shown in Fig. 1. It hosts a single Gd^{3+} ion and forms crystals with all molecules oriented in the same manner. In addition, magnetically diluted crystals can be grown by simply replacing Gd^{3+} with Y^{3+}, which is chemically equivalent but diamagnetic. This allows enhancing spin coherence times up to 2–3 μs [20] while keeping the possibility of orienting the magnetic fields $\vec{B}$ and $\vec{b}$

along specific molecular axes. This molecule shows a hard magnetic axis along the main molecular axis z. Its static spin Hamiltonian can be well described by Eqs. (1)–(3) with $S = 7/2$, $g = 2$, $D = 1281$ MHz, and $E = 294$ MHz. The overall splitting of the $d = 8$ multiplet is smaller than 1 K, or 20.8 GHz, thus ensuring that adjacent level splittings lie within the reach of conventional EPR as well as of other microwave technologies. In all calculations discussed below, we have chosen the static magnetic field $\vec{B}$ to point in the x direction (medium axis) and set $B = 0.15$ T. Under such conditions, the eigenstates of $\hat{H}_{ZF} + \hat{H}_{Zeeman}$ become close approximations to pure spin projections along $\vec{B}$. The time-dependent magnetic field $\vec{b}$ is perpendicular, and points in the y direction (easy axis), thus inducing transitions between adjacent energy levels.

B. Transition implementation via monochromatic pulses

In this section, we discuss the manipulation of the GdW$_{30}$ spin using monochromatic pulses resonant with the set of allowed transitions mentioned above and shown in Fig. 1. As an illustration, we consider the application of π pulses linking every two of these states. Figure 2 (top) displays the transformation infidelities (i.e., $1 - |\langle \psi(t_\pi^\lambda)|k\rangle|^2$) as a function of the time t_π^λ allocated to complete the operation, for the seven $|j\rangle \to |k = j + 1\rangle$ transitions. One can see that the error in the outcome state is reduced as $t_\pi^\lambda \to \infty$. In fact, from the logarithmic plot one may infer a quadratic behavior:

$$1 - |\langle \psi(t_\pi^\lambda)|k\rangle|^2 = \mathcal{O}((1/t_\pi^\lambda)^2). \tag{30}$$

It becomes clear that, in order to ensure a given fidelity, a minimum time (or, equivalently, a maximum amplitude) is required.

C. Optimization of state-to-state transitions

In this and the following section, we apply the QOCT methods described in Sec. II to quantum operations on GdW$_{30}$ having different targets. First, we optimize resonant transitions and sequences of these (in the next section we tackle the optimization of quantum gates). The goal here is to see how OCT permits the increase of the fidelities shown in Fig. 2 (top), by allowing for the presence in the pulse of other frequencies, besides the resonant one. We have performed QOCT calculations [65] considering, for each transition, the same total propagation time used to create Fig. 2 (top). Each of these propagation times t_π^λ corresponds to a π-pulse amplitude λ [Eq. (9)] that we have used now to set a bound for the Fourier expansion coefficients in the OCT maximization: the temporal shape of the microwave field is given by Eq. (20), where $|2u_j/\sqrt{t_\pi^\lambda}| \leq \lambda$. We have therefore used for this first set of calculations the first parameterization described in Sec. II C, i.e., Eq. (20).
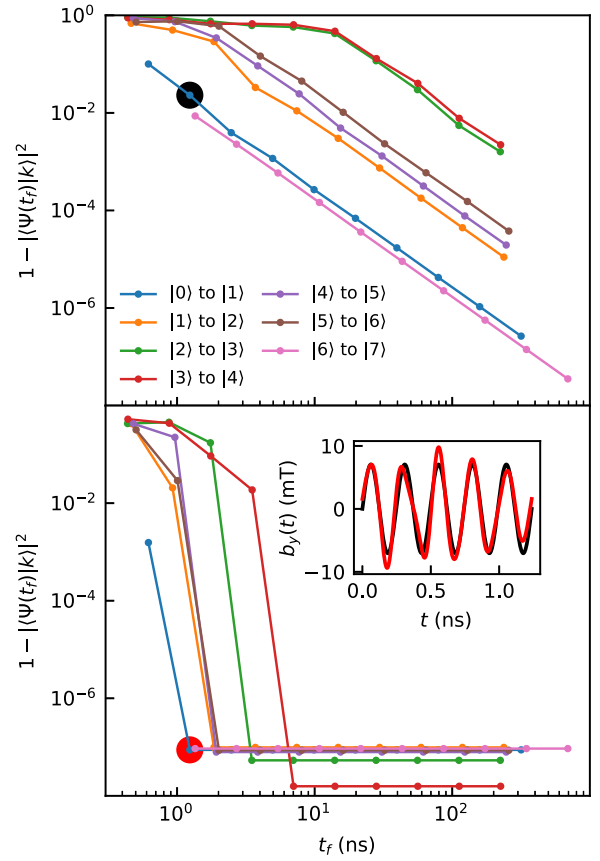

FIG. 2. Top: infidelities of the seven main resonant transitions in the GdW$_{30}$ molecule, as a function of the π-pulse time. Bottom: infidelities of the seven main transitions in the GdW$_{30}$ molecule, as a function of the total pulse time, for pulses obtained with optimal control. Inset: time-dependent shape of the pulses used to generate two of those $|0\rangle$ to $|1\rangle$ transitions: one π pulse (black) and one optimized pulse (red), corresponding to the black and red filled circles, respectively, on the blue lines.

Having in mind the level splitting present in GdW$_{30}$ and typical experimental capabilities, we have set the frequency cutoff at 8 GHz (the maximum frequency allowed in the parameter search space). The resulting (in)fidelities are displayed in Fig. 2 (bottom). The shaped pulses permit the decrease of those infidelities with respect to the simple π-pulse values down to negligible values for all but the shortest total transition times (we have set a 10^{-7} threshold to stop the search algorithm, and hence the flat curves for the longer times). In Fig. 2 (inset), we also compare the shape of control pulses corresponding to a resonant transition (monochromatic π pulse) and to the optimized one from states $|6\rangle$ to $|7\rangle$. These examples correspond to duration values marked respectively by black (top) and red (bottom) filled circles. It is clear that the optimized pulse achieves a much better fidelity in a much shorter time.

Let us now consider the more general case of optimizing transitions between states, say $|n\rangle$ and $|m\rangle$, that are not
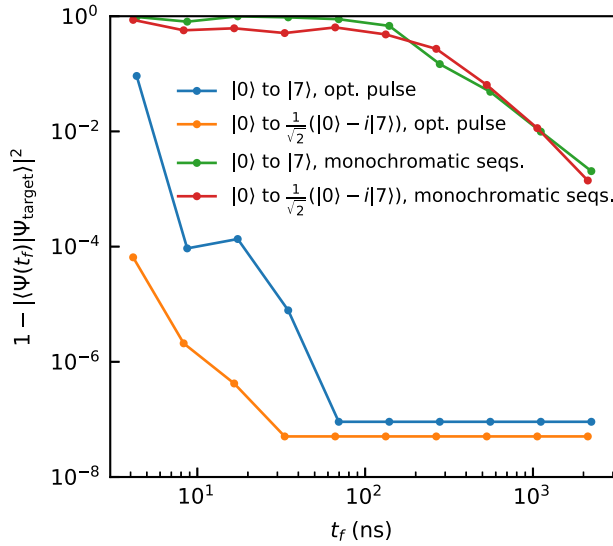
FIG. 3. Infidelities for the $|0\rangle \to |7\rangle$ and $|0\rangle \to (|0\rangle - i|7\rangle)/\sqrt{2}$ transitions, as a function of operation time, for the pulses obtained as a sequence of monochromatic resonant pulses (π or $\pi/2$), and for the optimal pulses obtained with QOCT.

directly coupled by the external field, i.e., $\langle n|S_y|m\rangle = 0$. A possible solution is to concatenate a series of π pulses, between intermediate states. In fact, this is a criterion for universality: if any two states can be connected through others, the qudit can perform any unitary and, in this sense, can be regarded as a universal quantum processor. However, the time needed is proportional to the number of pulses, which in practice is a limitation. Thus, in this case, QOCT offers a clear advantage by replacing a single shaped pulse to achieve, and accelerate, a process that would otherwise require a sequence of seven monochromatic pulses.

In Fig. 3 we have tested this by comparing the infidelity in the transition $|0\rangle \to |7\rangle$, using a sequence of π pulses between adjacent levels, $|k\rangle \to |k+1\rangle$, and using QOCT. The improvement is quite significant. In particular, we have run over a range of amplitudes λ that determine the π-pulse length for each transition, $t_\pi^\lambda(k \to k+1)$. The full $|0\rangle \to |7\rangle$ process then requires $t_f = \sum_{k=0}^{6} t_\pi^\lambda(k \to k+1)$. The plot displays the fidelity achieved with these pulse sequences. Then, for each of those times, we have performed QOCT calculations, once again setting a bound for the amplitudes of the individual Fourier terms equal to λ. The plot shows how, even at very short operation times, the fidelities achieved by the optimized pulses are almost equal to one. In terms of time scales, a 99% fidelity can be achieved in less than 10 ns, much shorter than $T_2 \simeq 2\,\mu$s, while reaching the same result with a sequence of monochromatic pulses would take more than 1 μs.

In Fig. 3 we also show results of a similar calculation, but using the $|0\rangle \to (|0\rangle - i|7\rangle)/\sqrt{2}$ state as target, a superposition state that can be reached with a $\pi/2$ pulse

corresponding to the $|0\rangle \to |1\rangle$ transition, followed by the same previous sequence of π pulses that raises the state through the next adjacent levels. The results are qualitatively similar to those obtained for the full $|0\rangle$ to $|7\rangle$ transition, thus showing that the speed enhancement achieved by the application of QOCT is not restricted to any particular class of transitions. This allows targeting the optimization of complex gates, which is discussed next.

We note that the pulses that have been optimized in this way to induce a given transition would also affect other states. This is in contrast with monochromatic pulses that only affect a given resonant transition. If one wishes to find an optimal, multifrequency pulse that only affects one transition, leaving all other states invariant, one would have to use the control method for the full evolution operator—as exemplified in the following section.

D. Quantum gate optimization

Finally, we proceed to our true objective: the search for nontrivial pulse shapes that realize quantum gates, with high fidelities, in short times. As target gates, we have chosen the family of Deutsch gates [66,67]

$$D(\theta) = \begin{bmatrix} I_6 & 0 & 0 \\ 0 & i\cos(\theta) & \sin(\theta) \\ 0 & \sin(\theta) & i\cos(\theta) \end{bmatrix}, \qquad (31)$$

where I_6 is the 6×6 identity matrix. Note that this family includes the Toffoli gate, for $\theta = \pi/2$. The reason for focusing on this set of gates is that it is universal: any circuit can be constructed by combination of these components.

These gates can be implemented with sequences of rotations induced with monochromatic pulses, but the necessary operation times may be inconveniently long. For example, following the procedure described in the Appendix, the Toffoli gate may be implemented through the sequence

$$D\left(\frac{\pi}{2}\right) = e^{i\pi/8} \hat{R}_Z^{(01)}\left(\frac{1}{4}\pi\right) \hat{R}_Z^{(12)}\left(\frac{1}{2}\pi\right) \hat{R}_Z^{(23)}\left(\frac{3}{4}\pi\right) \hat{R}_Z^{(34)}(\pi)$$
$$\times \hat{R}_Z^{(45)}\left(\frac{5}{4}\pi\right) \hat{R}_Z^{(56)}\left(\frac{3}{2}\pi\right) \hat{R}_Z^{(67)}\left(\frac{3}{4}\pi\right) \hat{R}_X^{(67)}(\pi). \qquad (32)$$

The global $e^{i\pi/8}$ factor is physically irrelevant. As discussed above, the rotations around the Z axis cannot be directly implemented in the experimental setup that we are considering, but can be substituted by X and Y rotations with the well-known composition $R_Z(\theta) = R_X(\pi/2)R_Y(\theta)R_X(-\pi/2)$. In this way, the final rotation tally is 22, which obviously translates into a very long operation time. In fact, if we set a minimum acceptable fidelity of 0.99 [using Eq. (14) as the fidelity measure],
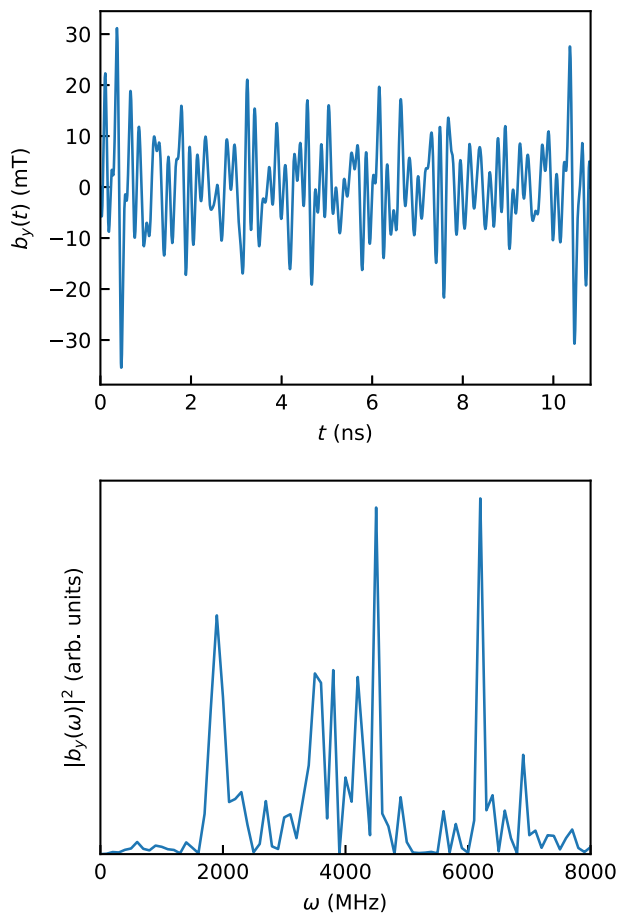
FIG. 4. Optimal pulse in the time domain (top) and its power spectrum in the frequency domain (bottom) of the optimal pulse obtained for the $\theta = \pi/4$ Deutsch gate. The pulse parameterization used is the simple Fourier expansion given by Eq. (20).

the required time is more than 4 μs, longer than the decoherence times of our experimental setup.

The use of multifrequency pulses obtained with QOCT appears then as a possible way to speed up the operation and make it feasible in practice. We have searched for solution pulses using the two different parameterizations discussed in Sec. II C, which amounts to assuming the existence of different types of experimental constraints.

In a first example we have used the simple Fourier parameterization given in Eq. (20), in combination with the per-frequency amplitude constraint given in Eq. (21). This means that the optimizations are performed constraining the allowed parameter set, such that each sinusoidal (or cosinusoidal) term in expansion (20) has a maximum amplitude. In the calculations shown here, we have set b_{max} to a relatively high value of 20 mT in order to make the operation, and therefore also the computational, times manageably short. However, we have performed
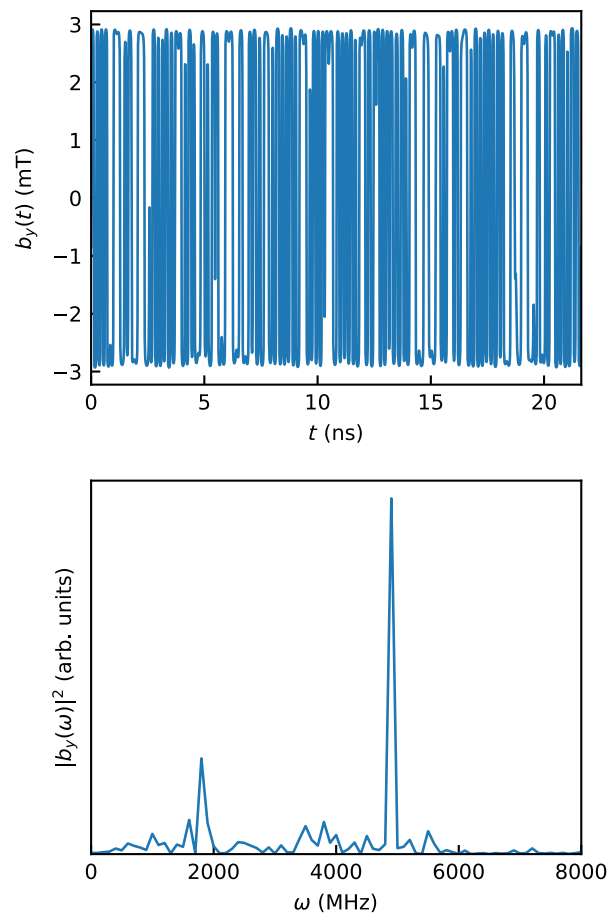

FIG. 5. Optimal pulse in the time domain (top) and its power spectrum in the frequency domain (bottom) of the optimal pulse obtained for the Toffoli ($\theta = \pi/2$ Deutsch) gate. The pulse parameterization used is that given by Eq. (22).

simulations with lower thresholds, and discuss below the influence of b_{max} on t_f.

The total propagation time t_f for this first example is set to 20 times the maximum natural period of the field-free Hamiltonian, i.e., the period corresponding to the smallest transition frequency. For the choice of static magnetic field used here ($\vec{B} = 0.15 T \vec{e}_x$), $t_f \sim 10$ ns. The optimization algorithm is an iterative process that we stop when the quality of the gate, measured as $F(\hat{U}(u;t_f)) = |\hat{U}(u,t_f) \cdot \hat{D}(\theta)|^2$, reaches a certain threshold, which for these calculations we have set to 0.99.

Figure 4 displays the results obtained for $\theta = \pi/4$ as an example (the results obtained for other angles are qualitatively similar). The top panel shows $f(u^{(0)};t)$ in real time, whereas the bottom panel displays its power spectrum. Both plots demonstrate the complexity of the pulses that do not have dominant frequencies.

The real-time evolution of the microwave field shows peaks of approximately 30 mT. Even though one can ensure in the algorithm that each frequency component is
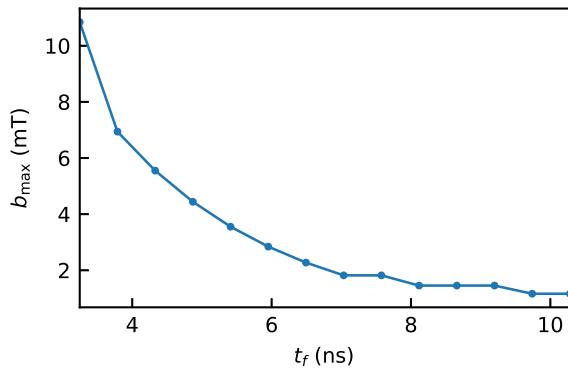
FIG. 6.   Minimal bound on the amplitudes (y axis) that allows us to obtain a $\theta = \pi/2$ Deutsch gate for a given total operation time (x axis).

below a fixed threshold, the real-time value is a sum of them all, and for this reason, it may surpass that bound. The experimental setup, however, may be limited by the amplitude of the field in real time, and not in frequencies, and for this reason, we have also implemented the parameterization defined in Eq. (22) that we used for our final sample calculation. In this case, the target is the Toffoli gate (the Deutsch gate with $\theta = \pi/2$), and we have enforced a b_{max} value of 3 mT. In this case, we required the operation time t_f to be longer, equal to 40 times the maximum natural period of the field-free Hamiltonian, or approximately 20 ns, in order to achieve the previously mentioned minimum fidelity of 0.99. The resulting optimal field, in both real time and in the frequency domain, is plotted in Fig. 5. It can be seen how the 3 mT amplitude bound is respected at all times.

In the previous examples, we set a total operation time t_f and an amplitude bound b_{max}. These two magnitudes are of course related: if, for a given t_f, we set a too low amplitude bound, the quality of the gate [as measured by Eq. (14)] will also be too low. In fact, if we fix a threshold for acceptable gate quality (say, 0.99) for each given propagation time, there will be a minimum amplitude bound necessary for the QOCT algorithm to return a successful pulse. Even with optimal pulse shapes, we need a sufficiently high field amplitude in order to get a high-quality gate. Whether this can be achieved depends on the given experimental setup chosen to implement the operations, and on its technical limitations.

We have therefore studied this issue by computing the minimum amplitude bound that can be used to constrain the QOCT calculation in order to get a given gate, as a function of operation time. The results are shown in Fig. 6. Those calculations are done with the first parameterization form that forces the amplitude bound to each frequency component, but of course a similar plot could be obtained with the second one. This type of plot helps us to ascertain whether or not the gate operations are experimentally

feasible, as in practice there is a hardware bound on the field amplitudes that can be used. Given this limit, one may learn from the plot what operation times are feasible, even with shaped optimal pulses. Obviously, the lower the available amplitudes, the longer the operation times must be.

IV. CONCLUSIONS

The previous results show that the use of complex pulses, engineered by optimal control techniques, provides a method for improving the speed of operations performed on spin qudits. The advantages are already noticeable for the realization of elementary transitions, when the application of monochromatic pulses is limited by the need of keeping the excitation amplitudes sufficiently low. Yet, they become even more important when dealing with more complex operations. Then, QOCT allows reaching any given fidelity of the outcome wave function with a single control pulse replacing the often long sequence of resonant pulses required by standard techniques. This possibility is especially relevant for algorithms that involve transitions between relatively disconnected states. For a necessarily limited coherence spin time, this difference can represent a big gain in the performance of such protocols.

The molecular qudit design and the way information is encoded on its spin states can be adapted to suit best the requirements of specific quantum protocols [18,68], thus offering a vast choice of possible molecular platforms and implementations. The optimal control techniques described in this work are flexible enough to be made compatible with almost any of them. Although we have here considered a specific molecule for illustrative purposes, QOCT can deal with any spin model and with diverse control interactions (e.g., magnetic or electric field pulses). Therefore, it can be adapted to boost the implementation of diverse algorithms. We feel that it will be of special relevance to quantum error correction, because reaching a fidelity improvement with such protocols critically depends on the ratio between the implementation time and T_2. With an additional computational cost, one can even consider optimizing the control pulses to best compensate for the actual sources of decoherence in each molecule, mainly dephasing by nuclear spins located in the ligand shell surrounding the magnetic core.

The use of more sophisticated control pulses represents a challenge to experimental implementations. Most commercial EPR systems work with relatively narrow excitation bands and a reduced choice of pulse shapes. In recent years such systems have been complemented with waveguide generators able to arbitrarily design the excitation pulses [69–71]. In addition, some systems allow the use of relatively high microwave field amplitudes [72]. Still, these setups are limited to frequencies lying sufficiently close to the cavity resonance frequency. In order to expand

the frequency window, one can resort to on-chip circuits, with the excitation being driven by an open transmission line. This scheme, illustrated in Fig. 1, has been applied to investigate coherent control of nitrogen-vacancy centers in diamond [73] and to perform broadband spectroscopy of GdW$_{30}$ and other molecular spin qudits [19,24]. It can also be used to read out the outcome, either by looking at the frequency-dependent absorption, in a projective measurement, or by coupling it to a superconducting resonator that can perform nondemolition, dispersive measurements of the qudit states [74]. Some experimental systems combining superconducting resonators and broadband control lines have recently been reported [75]. The main limitation of these systems is that microwave field amplitudes higher than 1–3 mT are difficult to achieve, on account of the bounds to the microwave power input associated with the attenuation of the input lines, which increases with frequency, and with the critical current density in the case of superconducting circuits [76]. Another promising implementation is based on the combination of single-molecule electronics with gates or coils able to locally generate arbitrarily shaped electric or magnetic microwave pulses. Experiments performed on molecules trapped between point contacts or between a metal substrate and a STM tip have provided measurements of spin coherence in individual molecules [77] and achieved the realization of Grover's search algorithm using three nuclear spin states in a Tb-based molecule [29]. One of the advantages of optimal control techniques is that they can easily incorporate bounds associated with experimental limitations, in either frequency of intensity of the time-dependent perturbation, and thus they provide the optimal control adapted to each specific situation.

In summary, the application of quantum optimal control theory to operate the states of molecular spin qudits offers remarkable prospects to improve their performance, compensating for their not too long coherence times. Equipped with these techniques, many more molecular systems and applications can become feasible, thus contributing to an alternative and promising path towards large-scale quantum computation and simulation.

APPENDIX: GENERATION OF UNITARY OPERATIONS

As has been stated in Sec. II B, one can decompose any unitary matrix $\hat{U} \in U(d)$ into a sequence of two-state rotations [such as those given by Eq. (6)], which can then be physically realized—albeit approximate—by monochromatic pulses. The technique behind this procedure is the QR decomposition algorithm with Givens rotations [57, 58]. A Givens rotation is defined as $\hat{G}^{(jk)} = \hat{g}^{(jk)} \oplus \hat{I}^{(\overline{jk})}$ with $\hat{g}^{(jk)}$ being a complex 2×2 unitary matrix. In our case,

$$\hat{g}^{(jk)} = \hat{R}_{\vec{n}}^{(jk)}(\theta) = \begin{bmatrix} c & s \\ -s^* & c \end{bmatrix} \quad (A1)$$

with $c = \cos(\theta/2)$, $s = -i\sin(\theta/2)e^{i\varphi}$, and $\varphi = \arg\mu_{jk} + \phi$. In the following, we refer to the complete matrix $\hat{G}^{(jk)} = \hat{R}_{\vec{n}}^{(jk)}(\theta) \oplus \hat{I}^{(\overline{jk})}$ as just $\hat{R}_{\vec{n}}^{(jk)}(\theta)$ to lighten the notation.

The algorithm determines a sequence of Givens rotations that transform the original unitary matrix into a diagonal matrix. Physically, each rotation operates on each pair of levels the original unitary dictates. The final diagonal matrix that we get accounts for the relative phases that arise between levels during the process. These phases can then be corrected with a final sequence of diagonal rotations ($\hat{R}_Z$ rotations).

Therefore, we apply a sequence of these rotations to the conjugate transpose of our problem matrix [78], $\hat{U}^\dagger$, and obtain the diagonal form

$$\hat{D} = \prod_l \hat{R}_{\vec{n}_l}^{(j_l k_l)}(\theta_l) \hat{U}^\dagger. \quad (A2)$$

Here, we take from each column c of $\hat{U}^\dagger$ the elements $(\hat{U}^\dagger)_{j_l c_l}$ and $(\hat{U}^\dagger)_{k_l c_l}$ $(j_l < k_l)$ and we use them to compute the rotation parameters, as shown in Algorithm 1 below. This algorithm proceeds by making zeros in the left-bottom corner of the matrix, until we end with the diagonal matrix $\hat{D}$. These rotations must obey the selection rules of our molecule. Usually, these rules follow a ladder-type coupling (connecting levels j and $j + 1$), which is why the algorithm takes that form for computing θ_l and $\vec{n}_l$.

The resulting diagonal matrix $\hat{D}$ can then be decomposed as a product of diagonal rotations:

$$\hat{D}^\dagger = \prod_m \hat{R}_Z^{(j_m k_m)}(\beta_m). \quad (A3)$$

This decomposition will consist of, at most, $d - 1$ rotations corresponding to $d - 1$ relative phases, β_m, as well as an extra global phase, β, which is physically irrelevant. If $\hat{R}_Z$ is not implementable in our experimental setup, we can generate it through three X and Y rotations, as mentioned in Sec. II B.

1: $\hat{V} \leftarrow \hat{U}^{\dagger}$
2: **for** $j = d,\ c = 0,\ j > c,\ c < d-1$ **do**
3:    $(r, c, s) \leftarrow \left(\sqrt{|U_{jc}|^2 + |U_{j-1c}|^2},\ U_{j-1c}/r,\ -U_{jc}/r \right)$
4:    $(\theta, \varphi) \leftarrow (2\arctan(|s/c|),\ \pi/2 + \arg[s] - \arg[c])$
5:    Store these parameters (θ, φ)
6:    $\hat{V} \leftarrow \hat{R}_{\vec{n}}^{(j-1,j)}(\theta)\hat{V}$
7: **end for**
8: $\hat{V} \leftarrow \arg[diag(\hat{V})]$
9: Solve

$$
\begin{bmatrix}
-1/2 & 0 & 0 & \dots & 0 & 1 \\
1/2 & -1/2 & 0 & \dots & 0 & 1 \\
0 & 1/2 & -1/2 & \dots & 0 & 1 \\
\vdots & \vdots & \vdots & \ddots & 0 & 1 \\
0 & 0 & 0 & \dots & -1/2 & 1 \\
0 & 0 & 0 & \dots & 1/2 & 1
\end{bmatrix}
\begin{bmatrix}
\beta_1 \\ \beta_2 \\ \beta_3 \\ \vdots \\ \beta_{d-1} \\ \beta
\end{bmatrix}
= \hat{V}
$$

10: Store these phases β_i

Algorithm 1. Unitary decomposition, adapted from Refs. [11, 57,58].

At the end, the unitary decomposition reads

$$
\hat{U} = e^{i\beta} \prod_m \hat{R}_Z^{(j_m k_m)}(\beta_m) \prod_l \hat{R}_{\vec{n}_l}^{(j_l k_l)}(\theta_l). \tag{A4}
$$

The procedure just explained is illustrated schematically as Algorithm 1, which is the algorithm used to derive Eq. (32) in the main text.

Several comments are relevant. First, the number of rotations required depends on the dimension, d, the structure of the unitary itself, $\hat{U}$, and on the connectivity between levels. Second, the decomposition is not unique. There may be alternative algorithms leading to different sequences. In fact, even the same algorithm may lead to a different rotation sequence, because some of the steps are very sensitive to the numerical precision of the calculations.

[1] F. Arute, *et al.*, Quantum supremacy using a programmable superconducting processor, Nature **574**, 505 (2019).

[2] Y. Wu, *et al.*, Strong Quantum Computational Advantage Using a Superconducting Quantum Processor, Phys. Rev. Lett. **127**, 180501 (2021).

[3] X. Xue, *et al.*, CMOS-based cryogenic control of silicon quantum circuits, Nature **593**, 205 (2021).

[4] D. Gottesman, A. Kitaev, and J. Preskill, Encoding a qubit in an oscillator, Phys. Rev. A **64**, 012310 (2001).

[5] M. N. Leuenberger and D. Loss, Quantum computing in molecular magnets, Nature **410**, 789 (2001).

[6] G. K. Brennen, D. P. O'Leary, and S. S. Bullock, Criteria for exact qudit universality, Phys. Rev. A **71**, 052318 (2005).

[7] S. Pirandola, S. Mancini, S. L. Braunstein, and D. Vitali, Minimal qudit code for a qubit in the phase-damping channel, Phys. Rev. A **77**, 032309 (2008).

[8] B. P. Lanyon, M. Barbieri, M. P. Almeida, T. Jennewein, T. C. Ralph, K. J. Resch, G. J. Pryde, J. L. O'Brien, G. Alexei, and A. G. White, Simplifying quantum logic using higher-dimensional Hilbert spaces, Nat. Phys. **5**, 134 (2009).

[9] E. Kiktenko, A. Fedorov, A. Strakhov, and V. Man'ko, Single qudit realization of the Deutsch algorithm using superconducting many-level quantum circuits, Phys. Lett. A **379**, 1409 (2015).

[10] R. Lapkiewicz, P. Li, C. Schaeff, N. K. Langford, S. Ramelow, M. Wieśniak, and A. Zeilinger, Experimental non-classicality of an indivisible quantum system, Nature **474**, 490 (2011).

[11] M. Ringbauer, M. Meth, L. Postler, R. Stricker, R. Blatt, P. Schindler, and T. Monz, A universal qudit quantum processor with trapped ions, ArXiv:2109.06903 (2021).

[12] S. Asaad, V. Mourik, B. Joecker, M. A. I. Johnson, A. D. Baczewski, H. R. Firgau, M. T. Madzik, V. Schmitt, J. J. Pla, F. E. Hudson, K. M. Itoh, J. C. McCallum, A. S. Dzurak, A. Laucht, and A. Morello, Coherent electrical control of a single high-spin nucleus in silicon, Nature **579**, 205 (2020).

[13] M. Neeley, M. Ansmann, R. C. Bialczak, M. Hofheinz, E. Lucero, A. D. O'Connell, D. Sank, H. Wang, J. Wenner, A. N. Cleland, M. R. Geller, and J. M. Martinis, Emulation of a quantum spin with a superconducting phase qudit, Science **325**, 722 (2009).

[14] D. Gatteschi and R. Sessoli, Quantum tunneling of magnetization and related phenomena in molecular materials, Angew. Chem. Int. Ed. **42**, 268 (2003).

[15] G. Aromí, D. Aguilà, F. Luis, S. Hill, and E. Coronado, Design of magnetic coordination complexes for quantum computing, Chem. Soc. Rev. **41**, 537 (2012).

[16] M. Atzori and R. Sessoli, The second quantum revolution: Role and challenges of molecular chemistry, J. Am. Chem. Soc. **141**, 11339 (2019).

[17] A. Gaita-Ariño, F. Luis, S. Hill, and E. Coronado, Molecular spins for quantum computation, Nat. Chem. **11**, 301 (2019).

[18] S. Carretta, D. Zueco, A. Chiesa, Á. Gómez-León, and F. Luis, A perspective on scaling up quantum computation with molecular spins, Appl. Phys. Lett. **118**, 240501 (2021).

[19] M. D. Jenkins, Y. Duan, B. Diosdado, J. J. García-Ripoll, A. Gaita-Ariño, C. Giménez-Saiz, P. J. Alonso, E. Coronado, and F. Luis, Coherent manipulation of three-qubit states in a molecular single-ion magnet, Phys. Rev. B **95**, 064423 (2017).

[20] M. J. Martínez-Pérez, S. Cardona-Serra, C. Schlegel, F. Moro, P. J. Alonso, H. Prima-García, J. M. Clemente-Juan, M. Evangelisti, A. Gaita-Ariño, J. Sesé, J. van Slageren, E. Coronado, and F. Luis, Gd-Based Single-Ion Magnets with Tunable Magnetic Anisotropy: Molecular Design of Spin Qubits, Phys. Rev. Lett. **108**, 247213 (2012).

[21] E. Moreno-Pineda, M. Damjanović, O. Fuhr, W. Wernsdorfer, and M. Ruben, Nuclear spin isomers: Engineering a Et$_4$N[DyPc$_2$] spin qudit, Angew. Chem. Int. Ed. **56**, 9915 (2017).

[22] E. Moreno-Pineda, C. Godfrin, F. Balestro, W. Wernsdorfer, and M. Ruben, Molecular spin qudits for quantum algorithms, Chem. Soc. Rev. **47**, 501 (2018).

[23] R. Hussain, G. Allodi, A. Chiesa, E. Garlatti, D. Mitcov, A. Konstantatos, K. S. Pedersen, R. De Renzi, S. Piligkos, and S. Carretta, Coherent manipulation of a molecular Ln-based nuclear qudit coupled to an electron qubit, J. Am. Chem. Soc. **140**, 9814 (2018).

[24] I. Gimeno, A. Urtizberea, J. Román-Roche, D. Zueco, A. Camón, P. J. Alonso, O. Roubeau, and F. Luis, Broad-band spectroscopy of a vanadyl porphyrin: A model electronuclear spin qudit, Chem. Sci. **12**, 5621 (2021).

[25] S. Chicco, A. Chiesa, G. Allodi, E. Garlatti, M. Atzori, L. Sorace, R. De Renzi, R. Sessoli, and S. Carretta, Controlled coherent dynamics of [VO(TPP)], a prototype molecular nuclear qudit with an electronic ancilla, Chem. Sci. **12**, 12046 (2021).

[26] F. Luis, A. Repollés, M. J. Martínez-Pérez, D. Aguilà, O. Roubeau, D. Zueco, P. J. Alonso, M. Evangelisti, A. Camón, J. Sesé, L. A. Barrios, and G. Aromí, Molecular Prototypes for Spin-Based CNOT and SWAP Quantum Gates, Phys. Rev. Lett. **107**, 117203 (2011).

[27] D. Aguilà, D. Barrios, V. Velasco, O. Roubeau, A. Repollés, P. Alonso, J. Sesé, S. Teat, F. Luis, and G. Aromí, Heterodimetallic [LnLn'] lanthanide complexes: Toward a chemical design of two-qubit molecular spin quantum gates, J. Am. Chem. Soc. **136**, 14215 (2014).

[28] J. Ferrando-Soria, E. Moreno-Pineda, A. Chiesa, A. Fernández, S. A. Magee, S. Carretta, P. Santini, I. Vitorica-Yrezabal, F. Tuna, E. J. L. McInness, and R. E. P. Winpenny, A modular design of molecular qubits to implement universal quantum gates, Nat. Commun. **7**, 11377 (2016).

[29] C. Godfrin, A. Ferhat, R. Ballou, S. Klyatskaya, M. Ruben, W. Wernsdorfer, and F. Balestro, Operating Quantum States in Single Magnetic Molecules: Implementation of Grover's Quantum Algorithm, Phys. Rev. Lett. **119**, 187702 (2017).

[30] F. Luis, P. J. Alonso, O. Roubeau, V. Velasco, D. Zueco, D. Aguilà, J. I. Martínez, L. A. Barrios, and G. Aromí, A dissymmetric [Gd$_2$] coordination molecular dimer hosting six addressable spin qubits, Commun. Chem. **3**, 176 (2020).

[31] E. Macaluso, M. Rubín, D. Aguilà, A. Chiesa, J. I. M. L. A. Barrios, P. J. Alonso, O. Roubeau, F. Luis, G. Aromí, and S. Carretta, A heterometallic [LnLn'Ln] lanthanide complex as a qubit with embedded quantum error correction, Chem. Sci. **11**, 10337 (2020).

[32] F. Tacchino, A. Chiesa, R. Sessoli, I. Tavernelli, and S. Carretta, A proposal for using molecular spin qudits as quantum simulators of light-matter interactions, J. Mater. Chem. C **9**, 10266 (2021).

[33] A. Chiesa, E. Macaluso, F. Petiziol, S. Wimberger, P. Santini, and S. Carretta, Molecular nanomagnets as qubits with embedded quantum-error correction, J. Phys. Chem. Lett. **11**, 8610 (2020).

[34] A. Chiesa, F. Petiziol, E. Macaluso, S. Wimberger, P. Santini, and S. Carretta, Embedded quantum-error correction and controlled-phase gate for molecular spin qubits, AIP Adv. **11**, 025134 (2021).

[35] C. Godfrin, R. Ballou, E. Bonet, M. Ruben, S. Klyatskaya, and W. W. F. Balestro, Generalized Ramsey interferometry explored with a single nuclear spin qudit, npj Quantum Inf. **4**, 53 (2018).

[36] K. Bader, D. Dengler, S. Lenz, B. Endeward, S.-D. Jiang, P. Neugebauer, and J. van Slageren, Room temperature quantum coherence in a potential molecular qubit, Nat. Commun. **5**, 5304 (2014).

[37] J. M. Zadrozny, J. Niklas, O. G. Poluektov, and D. E. Freedman, Millisecond coherence time in a tunable molecular electronic spin qubit, ACS Cent. Sci. **1**, 488 (2015).

[38] C. Brif, R. Chakrabarti, and H. Rabitz, Control of quantum phenomena: Past present and future, New J. Phys. **12**, 075008 (2010).

[39] S. J. Glaser, U. Boscain, T. Calarco, C. P. Koch, W. Köckenberger, R. Kosloff, I. Kuprov, B. Luy, S. Schirmer, T. Schulte-Herbrüggen, D. Sugny, and F. K. Wilhelm, Training Schrödinger's cat: Quantum optimal control, Eur. Phys. J. D **69**, 279 (2015).

[40] S. Conolly, D. Nishimura, and A. Macovski, Optimal control solutions to the magnetic resonance selective excitation problem, IEEE Trans. Med. Imaging **5**, 106 (1986).

[41] D. Rosenfeld and Y. Zur, Design of adiabatic selective pulses using optimal control theory, Magn. Reson. Med. **36**, 401 (1996).

[42] T. E. Skinner, T. O. Reiss, B. Luy, N. Khaneja, and S. J. Glaser, Application of optimal control theory to the design of broadband excitation pulses for high-resolution NMR, J. Magn. Reson. **163**, 8 (2003).

[43] N. Khaneja, T. Reiss, C. Kehlet, T. Schulte-Herbrüggen, and S. J. Glaser, Optimal control of coupled spin dynamics: Design of NMR pulse sequences by gradient ascent algorithms, J. Magn. Res. **172**, 296 (2005).

[44] M. Lapert, Y. Zhang, M. Braun, S. J. Glaser, and D. Sugny, Singular Extremals for the Time-Optimal Control of Dissipative Spin $\frac{1}{2}$ Particles, Phys. Rev. Lett. **104**, 083001 (2010).

[45] J. P. Palao and R. Kosloff, Quantum Computing by an Optimal Control Algorithm for Unitary Transformations, Phys. Rev. Lett. **89**, 188301 (2002).

[46] E. Brion, D. Comparat, and G. Harel, Implementation of a CNOT gate in two cold Rydberg atoms by the nonholonomic control technique, Eur. Phys. J. D **38**, 381 (2006).

[47] S. Schirmer, Implementation of quantum gates via optimal control, J. Mod. Opt. **56**, 831 (2009).

[48] D. M. Reich, M. Ndong, and C. P. Koch, Monotonically convergent optimization in quantum control using Krotov's method, J. Chem. Phys. **136**, 104103 (2012).

[49] S. Hou, L. Wang, and X. Yi, Realization of quantum gates by Lyapunov control, Phys. Lett. A **378**, 699 (2014).

[50] Y. Chou, S.-Y. Huang, and H.-S. Goan, Optimal control of fast and high-fidelity quantum gates with electron and nuclear spins of a nitrogen-vacancy center in diamond, Phys. Rev. A **91**, 052315 (2015).

[51] K. Arai and Y. Ohtsuki, Reduced-dynamics approach for optimally designing unitary transformations, Phys. Rev. A **92**, 062302 (2015).

[52] D. Dong, C. Wu, C. Chen, B. Qi, I. R. Petersen, and F. Nori, Learning robust pulses for generating universal quantum gates, Sci. Rep. **6**, 36090 (2016).

[53] S. Omanakuttan, A. Mitra, M. J. Martin, and I. H. Deutsch, Quantum optimal control of ten-level nuclear spin qudits in ^{87}Sr, Phys. Rev. A **104**, L060401 (2021).

[54] A. Wilson, E.-C. Yang, D. N. Hendrickson, and S. Hill, On the validity of the giant spin approximation and its application to single-molecule magnets, Polyhedron **26**, 2065 (2007), proceedings of the 10th International Conference on Molecule-based Magnets (ICMM 2006),

[55] S. Thiele, F. Balestro, R. Ballou, S. Klyatskaya, M. Ruben, and W. Wernsdorfer, Electrically driven nuclear spin resonance in single-molecule magnets, Science **344**, 1135 (2014).

[56] J. Liu, J. Mrozek, W. K. Myers, G. A. Timco, R. E. P. Winpenny, B. Kintzel, W. Plass, and A. Ardavan, Electric Field Control of Spins in Molecular Magnets, Phys. Rev. Lett. **122**, 037202 (2019).

[57] D. P. O'Leary and S. S. Bullock, QR factorizations using a restricted set of rotations, Electron. Trans. Numer. Anal. **21**, 20 (2005).

[58] D. P. O'Leary, G. K. Brennen, and S. S. Bullock, Parallelism for quantum computation with qudits, Phys. Rev. A **74**, 032334 (2006).

[59] L. S. Pontryagin, V. G. Boltyanskii, R. V. Gamkrelidze, and E. F. Mishechenko, *The Mathematical Theory of Optimal Processes* (John Wiley & Sons, New York/London, 1962).

[60] J. Johansson, P. Nation, and F. Nori, QuTiP: An open-source Python framework for the dynamics of open quantum systems, Comput. Phys. Commun. **183**, 1760 (2012).

[61] J. Johansson, P. Nation, and F. Nori, QuTiP 2: A Python framework for the dynamics of open quantum systems, Comput. Phys. Commun. **184**, 1234 (2013).

[62] A. Castro, *et al.*, Qocttools, https://acbarrigon.gitlab.io/qocttools/.

[63] D. Kraft, Algorithm 733: TOMP-Fortran modules for optimal control calculations, ACM Trans. Math. Softw. **20**, 262 (1994).

[64] S. G. Johnson, The NLopt nonlinear-optimization package, http://github.com/stevengj/nlopt.

[65] Note that the OCT for the simpler problem of state population—in contrast to the the harder problem of the creation of a given evolution operator or gate—requires equations that are slightly different to those described in Sec. II.

[66] D. E. Deutsch and R. Penrose, Quantum computational networks, Proc. R. Soc. London, A **425**, 73 (1989).

[67] X.-F. Shi, Deutsch, Toffoli, and CNOT Gates via Rydberg Blockade of Neutral Atoms, Phys. Rev. Appl. **9**, 051001 (2018).

[68] F. Petiziol, A. Chiesa, S. Wimberger, P. Santini, and S. Carretta, Counteracting dephasing in molecular nanomagnets by optimized qudit encodings, npj Quantum Inf. **7**, 133 (2021).

[69] M. Tseitlin, R. W. Quine, G. A. Rinard, S. S. Eaton, and G. R. Eaton, Digital EPR with an arbitrary waveform generator and direct detection at the carrier frequency, J. Magn. Reson. **213**, 119 (2011).

[70] P. E. Spindler, P. Schöps, A. M. Bowen, B. Endeward, and T. F. Prisner, in *eMagRes* (John Wiley & Sons, Ltd, 2016), p. 1477.

[71] T. F. Prisner, Shaping EPR: Phase and amplitude modulated microwave pulses, J. Magn. Reson. **306**, 98 (2019).

[72] P. A. S. Cruickshank, D. R. Bolton, D. A. Robertson, R. I. Hunter, R. J. Wylde, and G. M. Smith, A kilowatt pulsed 94 GHz electron paramagnetic resonance spectrometer with high concentration sensitivity, high instantaneous bandwidth, and low dead time, Rev. Sci. Instrum. **80**, 103102 (2009).

[73] G. de Lange, Z. H. Wang, D. Ristè, V. V. Dobrovitski, and R. Hanson, Universal dynamical decoupling of a single solid-state spin from a spin bath, Science **330**, 60 (2010).

[74] Á. Gómez-León, F. Luis, and D. Zueco, Dispersive Readout of Molecular Spin Qudits, Phys. Rev. Appl. **17**, 064030 (2022).

[75] A. K. Keyser, J. J. Burnett, S. E. Kubatkin, A. V. Danilov, M. Oxborrow, S. E. de Graaf, and T. Lindström, Pulsed electron spin resonance of an organic microcrystal by dispersive readout, J. Magn. Reson. **321**, 106853 (2020).

[76] M. D. Jenkins, U. Naether, M. Ciria, J. Sesé, J. Atkinson, C. Sánchez-Azqueta, E. d. Barco, J. Majer, D. Zueco, and F. Luis, Nanoscale constrictions in superconducting coplanar waveguide resonators, Appl. Phys. Lett. **105**, 162601 (2014).

[77] X. Zhang, C. Wolf, Y. Wang, H. Aubin, T. Bilgeri, P. Willke, A. J. Heinrich, and T. Choi, Electron spin resonance of single iron phthalocyanine molecules and role of their non-localized spins in magnetic interactions, Nat. Chem. **14**, 65 (2021).

[78] The sequence is applied to the conjugate transpose of the unitary so that, upon inversion, the unitary is written in terms of the sequence.